Thin Film Metallic Glasses: Preparations, Properties, and Applications

J.P. Chu, J.C. Huang, J.S.C. Jang, Y.C. Wang, and P.K. Liaw

With unique properties such as high strength, amorphous alloys in the bulk form have been a focus for many studies in recent years. Yet, the amorphous alloys (metallic glass) in the thin film form have not received much attention. In this paper, we will review and report some important and interesting results obtained from these thin film metallic glasses in which unique physical and mechanical properties can be enhanced by changing their compositions and by the precipitation of nanoscale particles.

INTRODUCTION

Metallic glasses, also called amorphous alloys, are homogeneous, isotropic, and free from crystalline defects. They have been studied extensively in the recent decade, particularly in the bulk shape.[1,2] These metallic glasses in the thin film form are also interesting to study because of their unique properties such as high strength and amorphous nature. Shimokohbe and his group had fabricated Pd-based ($Pd_{76}Cu_7Si_{17}$) and Zr-based ($Zr_{75}Cu_{19}Al_6$) thin film metallic glasses (hereafter abbreviated as TFMGs) first used in micro-electro-mechanical systems (MEMS).[3] Compared to conventional crystalline MEMS materials, TFMGs have structural advantages including, for example, high strength, absence of grain boundary and segregation. TFMGs are thus thought to have no size effect. The physical properties of TFMGs can be adjusted and mechanical properties can be enhanced by changing their compositions and by the precipitation of nanoscale particles.

In this paper, we will review and report some important and interesting results obtained from TFMGs in recent years.

How would you…

…describe the overall significance of this paper?

With unique properties such as high strength, absence of grain boundary and segregation, metallic glasses in the thin film form are a kind of amorphous alloy whose physical properties can be adjusted and mechanical properties can be enhanced by changing their compositions and by the precipitation of nanoscale particles. In this paper, we will review and report some important and interesting results obtained from related studies in recent years.

…describe this work to a materials science and engineering professional with no experience in your technical specialty?

Metallic glass thin films, having absence of grain boundary and segregation, have unique properties such as high strength and good ductility. This paper provides a review that reveals some important results and applications using this type of thin film. Examples include annealing-induced solid-state amorphization and the surface coating for fatigue property improvement.

…describe this work to a layperson?

With unique properties such as high strength, amorphous alloys in the bulk form have been a focus of many studies in recent years. Yet, the amorphous alloys (metallic glass) in the thin film form have not received much attention. In this paper, we will review and report some important and interesting results obtained from these thin film metallic glasses in which unique physical and mechanical properties can be enhanced by changing their compositions and by the precipitation of nanoscale particles.

THIN FILM METALLIC GLASSES: FABRICATION AND PROPERTIES

Fabrication

Physical vapor deposition (PVD) including sputtering and evaporation is one of the common procedures for fabricating TFMGs. One example is the Zr-based TFMG which is deposited by sputtering of a quaternary alloy target.[4–7] A broad Bragg peak in Figure 1 shows that this $Zr_{47}Cu_{31}Al_{13}Ni_9$ TFMG sputtered from an alloy target is mainly amorphous.[4] The tip of the Bragg peak hump at ~38 of 2θ indicates nanocrystalline phases dispersed in the amorphous matrix, as confirmed by the transmission electron microscopy (TEM) result. An example of a TEM bright-field image with a halo ring selected area diffraction (SAD) pattern in Figure 2, obtained from a sputtered $Zr_{61}Al_{7.5}Ni_{10}Cu_{17.5}Si_4$ TFMG, reveals a typical homogeneous amorphous matrix with dispersed nanocrystallites.[7] Since the sputter deposition is considered to be a non-equilibrium process, it becomes a useful route to obtain the amorphous structure.

To examine the mixing and vitrification behavior, binary Zr-Cu, Zr-Ti[8] and Mg-Cu thin films are prepared by co-sputtering of elemental targets.[9] Figure 3 shows that the co-sputtered Zr-Cu and Mg-Cu films, with various intermetallic compounds in the Zr-Cu equilibrium phase diagram, are found to be amorphous, suggesting the high vitrification tendency and good glass-forming ability.[8,9] It is also suggested that the composition window for achieving fully amorphous thin films is much wider than that for the BMGs. For example, the ternary Zr-Cu-Ti system,

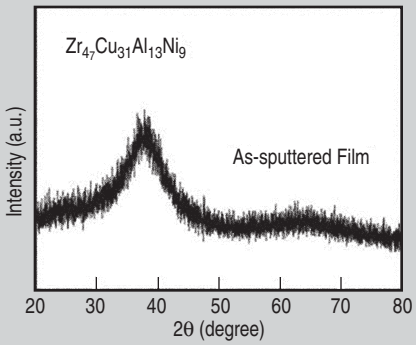

Figure 1. XRD pattern of the Zr-based TFMG with 1 μm thickness.[4]

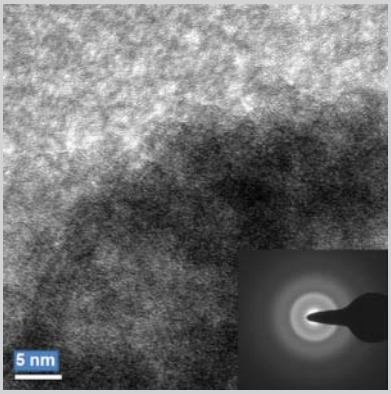

Figure 2. Plane-view bright-field transmission electron microscopy (TEM) image of the Zr-based TFMG with selected area diffraction pattern revealing a homogeneous amorphous matrix with dispersed nanocrystallites.[7]

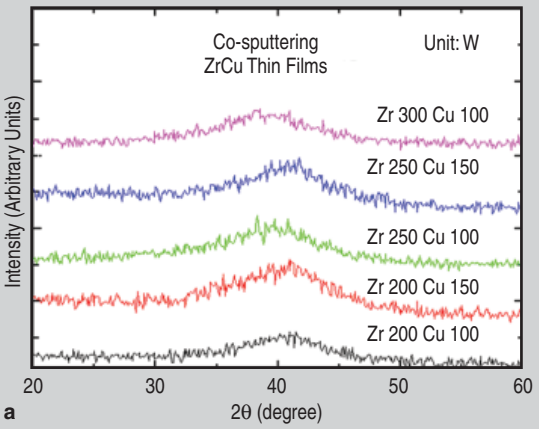

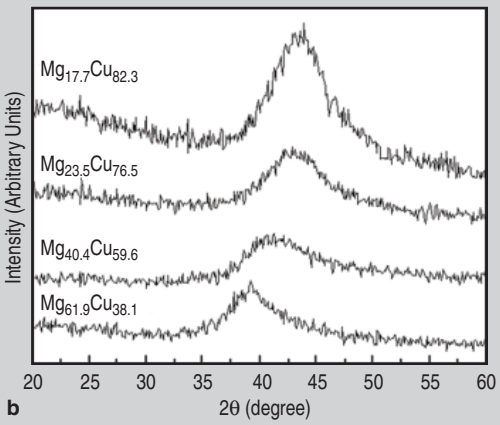

Figure 3. Typical x-ray diffraction patterns for the binary (a) Zr-Cu, and (b) Mg-Cu thin films by co-sputtering of elemental targets.[8,9]

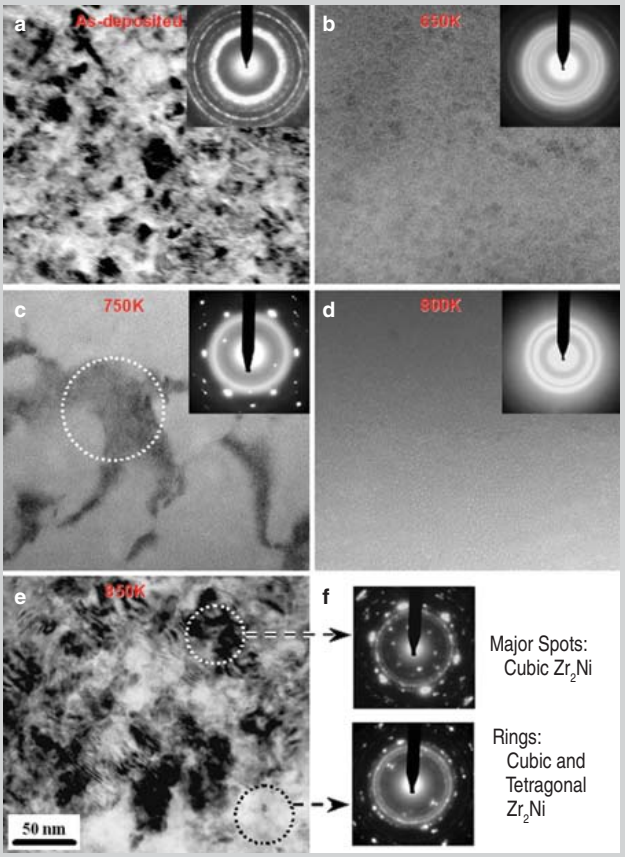

Figure 4. Plane-view TEM micrographs and diffraction patterns of the Zr-based TFMG in (a) as-deposited and annealed conditions at (b) 650, (c) 750, (d) 800, and (e) 850 K. The circled regions indicate the locations for obtaining the diffraction patterns.[4]

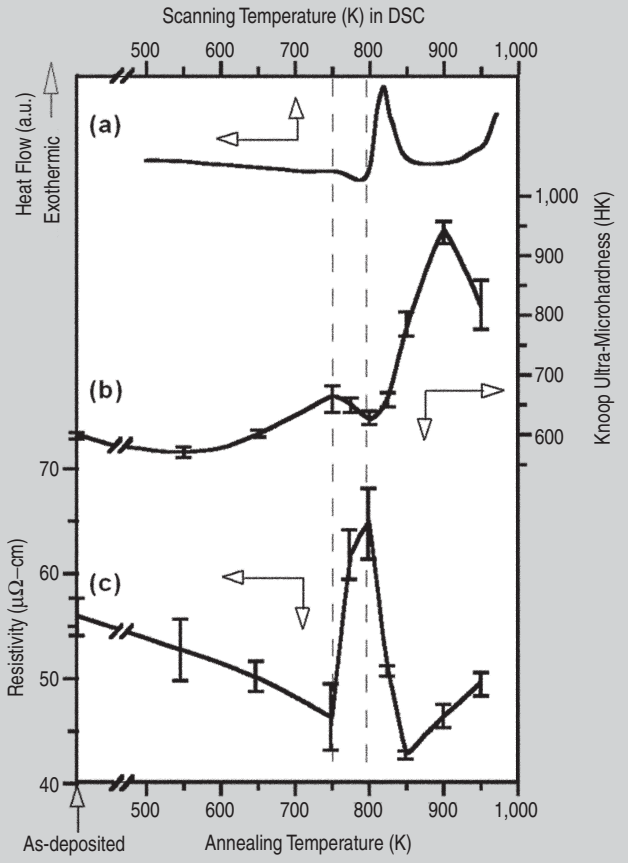

Figure 5. Variations of electrical resistivity and hardness of a Zr-based TFMG with annealing temperature. DSC thermogram is included for comparison.[4]

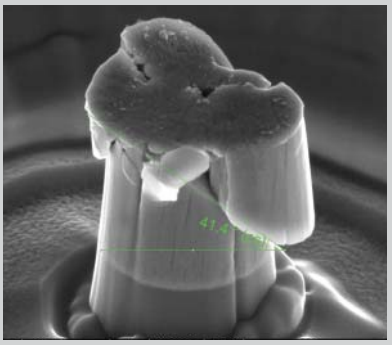

Figure 6. SEM micrograph of a micropillar prepared from Cu-based TFMG annealed at 723 K in ΔT and deformed under a strain rate of 1×10^{-3} s^{-1}.

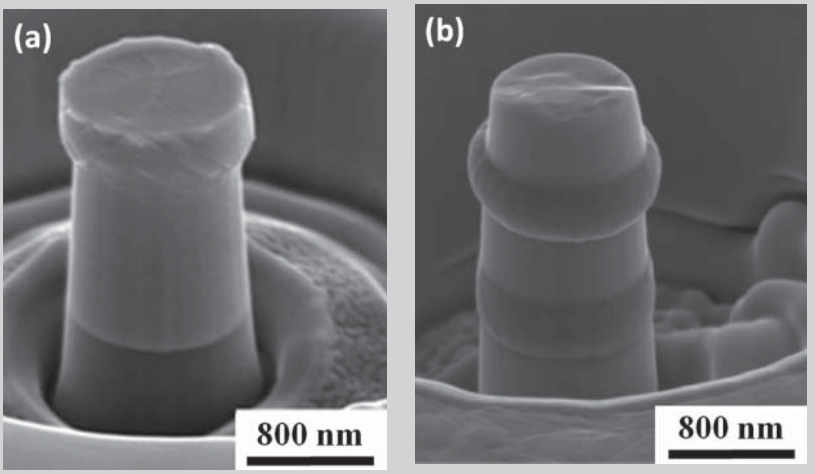

Figure 7. Micropillars: (a) Zr-based TFMG on the top, originally 550 nm in height, compressed to ~280 nm (or 50–55% compression strain), with a thick Zr underlayer. (b) Zr-based TFMG remains basically undeformed, with a soft Cu underlayer heavily deformed.[15]

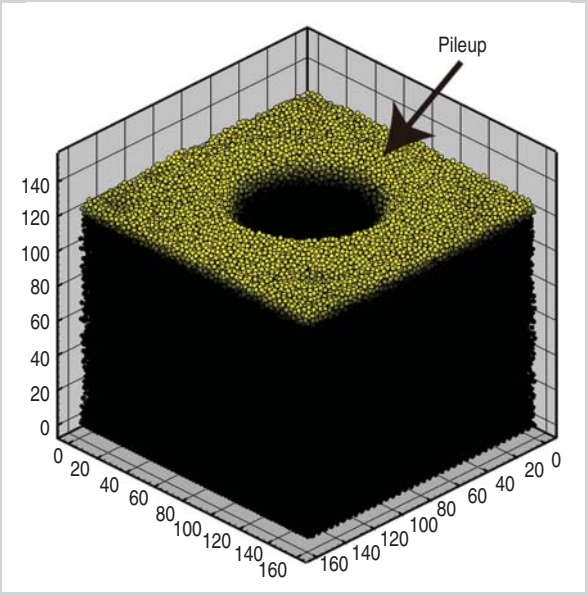

Figure 8. Molecular-dynamics model (about 200,000 atoms), obtained from sputter deposition simulations, for studying the indentation behavior of the Zr-based metallic-glass film, indented with a diamond conical tip. A pileup around the indent is observed due to the homogeneous flow.

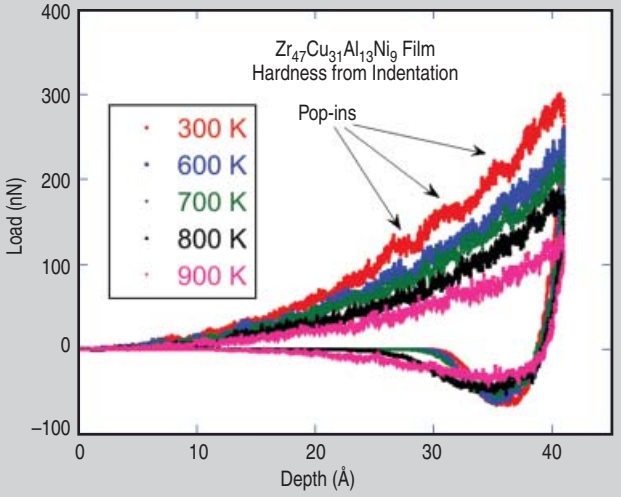

Figure 9. Indentation load-displacement curves at various temperatures for the $Zr_{47}Cu_{31}Al_{13}Ni_9$ TFMG from the 40 Å-thick MD model. A negative force indicates the adhesion between the film and indenter during unloading.

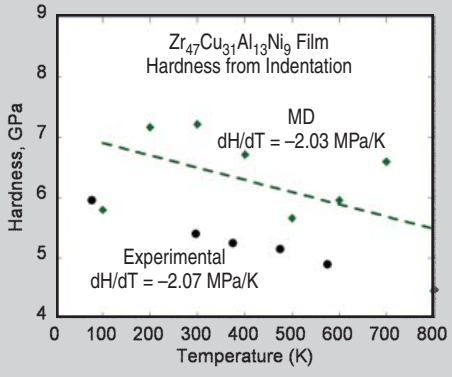

Figure 10. Hardness vs. temperature verification between simulation (◆) and experiment (●).

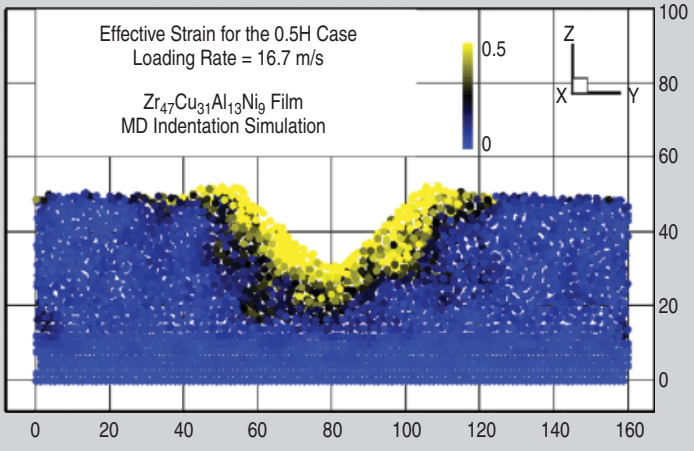

Figure 11. Atomic strain at the indentation depth of a half of the film thickness (labeled as the 0.5H case). The displacement loading rate was 16.7 m/s. Shear banding patterns can be observed around the indent.

particularly with high Ti contents, is normally difficult to be fully vitrified in the bulk form. However, one can obtain amorphous Zr-Cu-Ti thin films with an excessive Ti content as high as 19% by co-sputtering of elemental targets.[10]

Properties

A thorough knowledge of thermal, physical, and mechanical properties is essential for the further applications of TFMGs. For instance, the thermal stability of the amorphous phase of TFMGs is important for the microforming and annealing processes. It has been reported that partially crystallized TFMGs transform into various nanoscale and amorphous structures during the annealing before the extensive crystallization takes place in Zr-,[4] Fe-,[11] and Cu-based[12] TFMGs. Crystalline phases are more thermodynamically favorable than metastable phases formed in the as-deposited condition.[13] In some elementally modulated crystalline films, solid-state amorphization (SSA) within the interfacial nanometer regions could occur through annealing-induced diffusion reactions.[14]

Annealing of sputtered metastable TFMGs is found to yield the formation of various nanoscale and amorphous structures, thus resulting in changes of electrical and mechanical properties. These property changes are significant when annealed in the supercooled liquid region (ΔT), defined by the temperature range, $\Delta T = T_x - T_g$, where T_g is the glass transition temperature and T_x is the crystallization temperature. To determine T_g, T_x, and other thermal properties, the differential scanning calorimeter (DSC) is used. For the Zr-based ($Zr_{47}Cu_{31}Al_{13}Ni_9$) TFMG, T_g and T_x temperatures are 758 K and 797 K, respectively, with a ΔT of approximately 40 K.[4] As the film is annealed in ΔT, the annealing-induced amorphization occurs as shown in Figure 4.[4] Transmission electron microscopy images show a series of structural changes at different annealing temperatures. The film is completely amorphous at 800 K in ΔT as indicated in the microstructure and diffraction pattern. The amorphization in ΔT yields film property changes such as surface roughness, hardness, and electrical resistivity (Figure 5[4]). For instance, the surface roughness decreases from 0.690 nm in as-deposited state to 0.414 nm in ΔT. Fe- and Cu-based films also exhibit annealing-induced amorphization in ΔT.[11,12] Low free energy of the amorphous phase with sufficient thermal and interfacial energies between nanocrystallites and glassy matrices could be considered as the driving force for the vitrification during annealing in ΔT region. The large negative heat of mixing and hence the low free energy of the amorphous phase can be related to the amorphization induced by annealing.[4]

For the mechanical property evaluations, nano-hardness is commonly used. For the ternary $Zr_{52}Cu_{29}Ti_{19}$ TFMG, sub-T_g annealing of the film induces the formation of medium-range-ordered clusters and the nano-hardness is increased by 35% to 6.6 GPa.[10] The micropillars with aspect ratios >1.5 (1,600 nm height and 980 nm in diameter) were milled by focused ion beam (FIB) from a quaternary $Cu_{51}Zr_{42}Al_4Ti_3$ TFMG to study the effects of individual structure arising from different annealing temperatures. The nanoindention results of micropillar exhibit that the compression yield stress increases from 3.7 GPa in the as-deposited state to maximum 4.6 GPa at 723 K in ΔT, followed by a decrease to 3.8 GPa at 798 K above T_x. In another Cu-based TFMG, the nano-hardness can reach maximum ~9 GPa in ΔT compared with ~7.6 GPa of sub-T_g annealed sample at 698 K.

A thorough knowledge of thermal, physical, and mechanical properties is essential for the further applications of TFMGs.

The SEM image shown in Figure 6 is a typical micropillar failed by a single major shear band with the plane of shear yielding about 41.4 , which indicates the metallic materials in both thin film and bulk forms have the similar fracture character. Yet, it is worth mentioning that for the TFMG, the positive dependence of hardness with temperature is unique and distinct from annealing-induced softening of conventional materials.

Furthermore, multilayered TFMGs are getting more attention lately. A recent work demonstrates that the brittleness of a ZrCu metallic glass coating can be alleviated by placing a nanocrystalline metallic Zr underlayer.[15] The brittle TFMG on the top of the micropillar becomes highly ductile and exhibits a plastic strain over 50% at room temperature, as shown in Figure 7a.[15] The nanocrystalline Zr layer acts like a buffer to effectively dissipate the kinetic energy carried by incident shear bands. Nano-twinning was induced in the nanocrystalline Zr layer. However, the metallic underlayer must be sufficiently thick to be able to resist the incident shear bands. The thickness of the crystalline layer would be dependent upon the strength of the amorphous and crystalline layers. It is also found that this underlayer needs to be sufficiently strong. When the nanocrystalline Zr underlayer is replaced by a softer nanocrystalline Cu layer, no apparent deformation occurs in the TFMG top layer. Instead, the softer Cu layer would be deformed plastically, as depicted in Figure 7b.[15] These results suggest the life span of a brittle amorphous layer can be improved by using an appropriate metallic underlayer.

SIMULATION

To understand amorphous structure formation during deposition and deformation behavior under indentation, molecular-dynamics (MD) models of the Zr-based metallic-glass film ($Zr_{47}Cu_{31}Al_{13}Ni_9$) by simulating sputter deposition were constructed. The as-deposited films were further used for the subsequent nano-indentation simulations.

A thermal-control-layer-marching algorithm[16] was adopted to accelerate the deposition. Without the algorithm, the computation for depositing a relatively thick film is time-consuming. From this simulated deposition, the interface between the film and substrate is considered to be "naturally" formed, based on the MD principles. Figure 8 shows the results of the deposited Zr-

$_{47}Cu_{31}Al_{13}Ni_9$ film via the MD simulation with an indent. It can be seen that pileup occurs around the indent, indicating the homogeneous flow of the metallic glass under an intensive stress around the indenter. In the deposition and indentation simulations, interatomic potentials that are derived from the many-body, tight-binding second-moment approximation (TB-SMA),[17] were adopted to simulate the interactions among the four species of atoms forming the metallic glass.

In Figure 9, indentation load-displacement curves are shown at various temperatures. Negative force indicates the attraction between the tip and the surface of the film due to the weak interaction, while the tip is retracting from the sample. The adhesion force may provide valuable information about the surface energy of the film in such a small dimension. As the temperature increases, the stiffness of the material decreases. Moreover, the maximum load, corresponding to the same indentation depth, also decreases, indicating the softening of the material at high temperatures. At the 300 K case, the serrated flow in the load-displacement curve may be evident of the shear-band activation or shear transformation in the shear transformation zone (STZ).[18] The pop-in depth is about 2.5 Å, considerably smaller than what has been reported in the literature, due to the large displacement rate used in MD. At higher temperatures, the pop-in phenomenon is not clearly observed, consistent with experiments.[18]

Using the definition of hardness, namely the ratio between the maximum load and the projected area, the hardness of the film calculated from the MD simulation is summarized in Figure 10. Based on our in situ indentation calculations at various temperatures (labeled as solid diamonds in the figure), the hardness values of the metallic-glass film decrease from about 7 GPa to about 5 GPa with the increase of temperature from 100 K to 800 K. The dashed line indicates the linear curve fit of the MD data. The scattering of MD data is due to noise in the force calculation in MD. It is found that the magnitude and decreasing rate of the hardness, about 2 MPa/K, with respect to the temperature are in agreement between MD calculations and experiments. The experimental data (labeled as solid circles) are from Reference 19 for $Zr_{55}Cu_{30}Al_{10}Ni_5$ in at.% (T_g = 680 K). Note that this composition is slightly different from the one used in the MD calculations. Note, due to the high loading rates in the MD simulation, the higher hardness from calculations may reflect the time-dependent behavior of the system. Experimental measurables, such as the pileup index,[20] have been be used to verify the computer simulation. The comparison between the experiment and simulation shows a good agreement for the indentation depth much less than the film thickness. For deep indents, the substrate effects make the Oliver–Pharr method inaccurate.

The effective strains are shown in Figure 11 for the half-thickness indentation depth (labeled as the 0.5H case). The displacement loading rate was 16.7 m/s. Note that the substrate, appearring as a regular lattice, has a thickness of 4 Å. Atomic strains can be calculated from the atom positions at a given time via a discrete deformation gradient tensor.[21] The effective strains are calculated with the von-Mises-type formula. Radial shear bands (dark regions extending from the indents) can be observed. The yellow regions are of high strain, where plastic flows occur. Other dark spots in the film are residual strains, resulting from the deposition. It can be seen that increasing loading rates cause larger plastic-flow regions. A larger plastic zone indicates less reaction forces that the zone can provide. Hence, the hardness decreases when the loading-rate increases, consistent with the experiment.[19]

The connections between STZs and the atomic shear banding can be understood as that at the beginning of the indentation, STZ may be activated at the 'weak spots' (defined as regions with atoms loosely packed from deposition) around the indent with some loading, and embryonic shear bands may form afterwards due to time-dependent properties or continuous loading. With increases of the loading, embryonic shear bands may propagate, and form shear bands eventually. However, the original weak spots where first shear transformations took place may become a part in the plastic-flow regions due to further loading. Moreover, during the propagation of shear bands, other weak spots in the material may go through the shear transformation when the effective strain reaches a critical value on the order of 0.01 or smaller (the dark regions in Figure 11).

APPLICATIONS

In addition to the MEMS applications, some TFMG applications have been explored recently. With the deposition of a 200-nm thick $Zr_{47}Cu_{31}Al_{13}Ni_9$ TFMG, the fatigue life of the 316L stainless steel is increased by 30 times, while the fatigue limit is elevated by 30%, as shown in Figure 12,[5] depending on the maximum stress applied to the steel. This is the first demonstration that confirms the TFMG has a similar property to that of conventional hard coating materials (e.g., TiN) for the fatigue property improvements. Such property improvements by TFMG are attributed to many factors, including the high strength, ductile in thin film form, compressive residual stress, good adhesion between the substrate and film to impede the crack initiation and propagation. The smooth surface after the TFMG coating (4.81 nm vs. 2.55 nm of uncoated and coated surface roughness, respectively) is also thought to reduce the nucleation sites for crack initiation on the surface.

Unlike copper and its alloys, brass and bronze, that are naturally antimicrobial materials, the TFMGs are found to be useful for the potential antimicrobial application by exhibiting much better hydrophobic properties due to their amorphous surface nature. For instance, the wetting angles of TFMG-coated and 304 stainless steel substrates are 92 and 46 , respectively. Antimicrobial activity test results further reveal that the Zr-based TFMG exhibits beneficial antimicrobial effects on some microbes, such as Escherichia coli and Pseudomonas aeruginosa, as shown in Figure 13.[22] Therefore, the TFMG is promising for improving the antimicrobial properties of substrates in the medical application. In addition, the TFMG similar to the 304 stainless steel possessing better corrosion resistance without any localized pitting corrosion after the polarization test (Figure 14[7]). Moreover, the AC impedance test re-

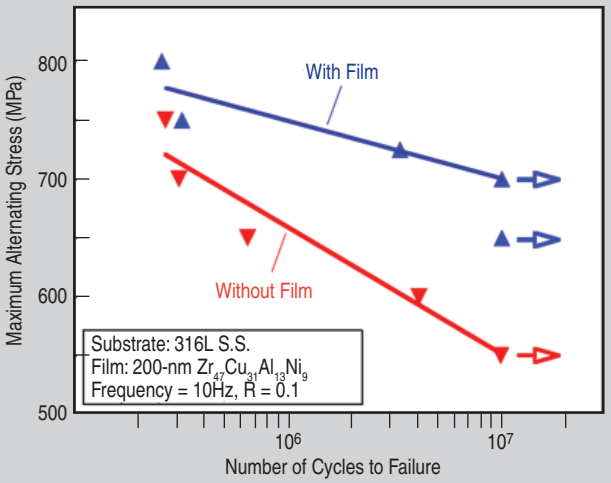

Figure 12. Stress versus fatigue life cycle for 316L stainless steel with and without the Zr-based TFMG. Arrows indicate the run-out data without the failure.[5]

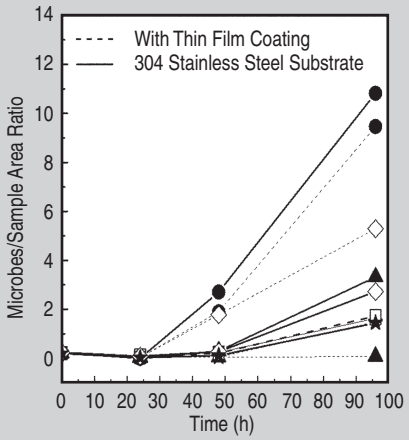

Figure 13. Microbes/sample area ratio as a function of incubation time for different microbes grown on M-H agar plate. Escherichia coli (▲), Staphylococcus aureus (□), Pseudomonas aeruginosa (●), Acinetobacter baumannii (◇), and Candida albicans (★).[22]

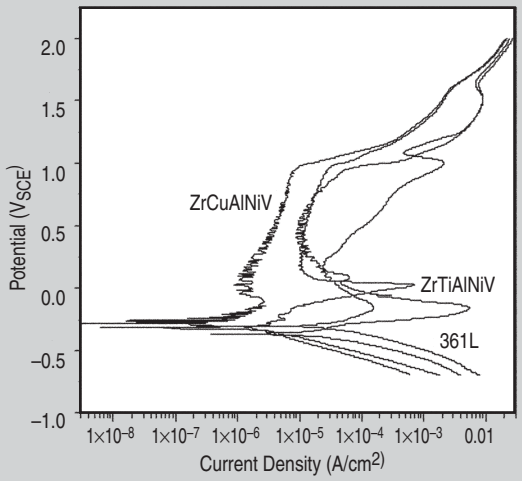

Figure 14. Analysis results of polarization curves of 316L stainless steel and TFMGs based on ZrCuAlNiV, and ZrTiAlNiV.[7]

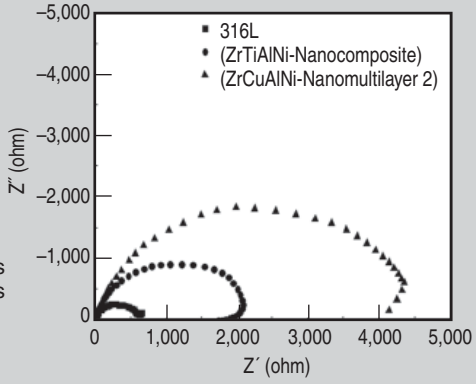

Figure 15. AC impedance test results of 316L stainless steel and two TFMGs based on ZrCuAlNiV and ZrTiAlNiV.[7]

sult reveals that the impedance value of TFMG is superior to that of 316L stainless steel (Figure 15[7]), implying that the TFMG has a better corrosion resistance owing to its amorphous state.

ACKNOWLEDGEMENTS

Many hard-working students and research associates are gratefully acknowledged for their contributions. This work is supported by National Science Council of Republic of China, Taiwan, under NSC 98-2221-E-011-037-MY3 and 96-2218-E-110-001.

References

1. M.W. Chen, *Annu. Rev. Mater. Res.,* 38 (2008), p. 445.
2. J.C. Huang, J.P. Chu, and J.S.C. Jang, *Intermetallics,* 17 (2009), p. 973.
3. Y. Liu et al., *Proceedings of the 14th IEEE International Conference on Micro Electro and Mechanical Systems* (Piscataway, NJ: IEEE, 2001), pp. 102–105.
4. J.P. Chu, et al., *Phys. Rev. B,* 69 (2004), p. 113410.
5. C.L. Chiang et al., *Appl. Phys. Lett.,* 88 (2006), p. 131902.
6. F.X. Liu et al., *Mater. Mater. Sci. Eng. A,* 468–470 (2007), p. 246.
7. C.W. Chu et al., *Thin Solid Films,* 517 (2009), p. 4930.
8. C.J. Chen et al., *J. Alloys Compounds,* 483 (2009), p. 337.
9. H.S. Chou et al., *J. Alloys Compounds,* 483 (2009), p. 341.
10. H.S. Chou et al., *Appl. Phys. Lett.,* 93 (2008), p. 191901.
11. J.P. Chu et al., *Appl. Phys. Lett.,* 88 (2006), p. 012510.
12. J.P. Chu, *JOM,* 61 (1)(2009), p. 72.
13. J.P. Chu et al., *J. Appl. Phys.,* 88 (2000), p. 6086.
14. R.B. Schwarz and W.L. Johnson, *Phys. Rev. Lett.,* 51 (1983), p. 415.
15. M.C. Liu et al., *Scripta Mater.,* 61 (2009), p. 840.
16. H.C. Lin et al., *P. Roy. Soc. A,* 461 (2005), p. 3977.
17. F. Cleri and V. Rosato, *Phys. Rev. B,* 48 (1993), p. 22.
18. C.A. Schuh and T.G. Nieh, *Acta Mater.,* 51 (2003), p. 87.
19. V. Keryvin et al., *Philos. Mag.,* 88 (2008), p. 1773.
20. F.X. Liu, Y.F. Gao, and P.K. Liaw, *Metall. Mater. Trans. A,* 39 (2008), p. 1862.
21. P.M. Gullett et al., *Model. Simul. Mater. Sci. and Eng.,* 16 (2007), p. 01500.
22. P.T. Chiang et al., accepted for publication in *Fooyin Journal of Health Sciences.*

J.P. Chu is with the Department of Polymer Engineering and Graduate Institute of Engineering, National Taiwan University of Science and Technology, Taipei, Taiwan 10607; J.C. Huang is with the Department of Materials Science and Optoelectronic Science, Center for Nanoscience and Nanotechnology, National Sun Yat-Sen University, Kaohsiung 80424, Taiwan; J.S.C. Jang is with the Department of Mechanical Engineering and Institute of Materials Science and Engineering, National Central University, 300 Chung-Da Rd. Chung-Li 32001, Taiwan; Y.C. Wang is with the Department of Civil Engineering, National Cheng Kung University, Tainan 70101, Taiwan; and P.K. Liaw is with the Department of Materials Science and Engineering, University of Tennessee, Knoxville, TN 37996-2200, USA.